NANO LETTERS

Letter

pubs.acs.org/NanoLett

Graphene as a Promising Electrode for Low-Current Attenuation in Nonsymmetric Molecular Junctions

Qian Zhang,[†,§] Longlong Liu,[∥] Shuhui Tao,[†,§] Congyi Wang,[†] Cezhou Zhao,[‡] César González,[⊥,#] Yannick J. Dappe,[⊥] Richard J. Nichols,[§] and Li Yang*[,†,§]

[†]Department of Chemistry and [‡]Department of Electrical and Electronic Engineering, Xi'an-Jiaotong Liverpool University, Suzhou, Jiangsu, 215123 China

[§]Department of Chemistry, University of Liverpool, Liverpool, L69 7ZD U.K.

[∥]Department of Chemistry and Chemical Engineering, Chongqing University, Chongqing, 400030, China

[⊥]SPEC, CEA, CNRS, Université Paris-Saclay, CEA Saclay 91191 Gif-sur-Yvette Cedex, France

[#]Departamento de Electrónica y Tecnología de Computadores, Universidad de Granada, Campus de Fuente Nueva & CITIC, Campus de Aynadamar 18071, Granada, Spain

Supporting Information

ABSTRACT: We have measured the single-molecule conductance of 1,*n*-alkanedithiol molecular bridges (n = 4, 6, 8, 10, 12) on a graphene substrate using scanning tunneling microscopy (STM)-formed electrical junctions. The conductance values of this homologous series ranged from 2.3 nS (n = 12) to 53 nS (n = 4), with a decay constant β_n of 0.40 per methylene ($-CH_2$) group. This result is explained by a combination of density functional theory (DFT) and Keldysh–Green function calculations. The obtained decay, which is much lower than the one obtained for symmetric gold junctions, is related to the weak coupling at the molecule–graphene interface and the electronic structure of graphene. As a consequence, we show that using graphene nonsymmetric junctions and appropriate anchoring groups may lead to a much-lower decay constant and more-conductive molecular junctions at longer lengths.

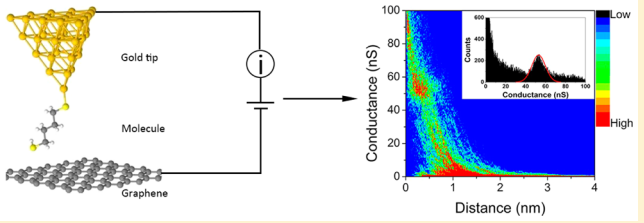

KEYWORDS: *Graphene-based electrode, single molecule conductance, charge transport, alkanedithiol, density functional theory*

Although technologically relevant molecular electronic devices still seem a long way off, the ability to measure the electrical properties of single molecules can be now achieved with a variety of techniques that were not available at the genesis of the field.[1] The ability to construct robust and reproducible molecular junctions, both for large-area planar contacts and at the single-molecule level, and to reliably characterize their electrical properties has been a key driver of the field of molecular electronics over the past decade.[2] In particular, the development of techniques using, for example, mechanically controlled break junctions (MCBJ), scanning tunneling microscopy break junctions (STM-BJ), conductive probe atomic force microscopy (CP-AFM) and the $I(s)$ technique (I = current, s = vertical distance) based on STM[3−6] have given new understanding and control of the flow of current through molecules.[7] These techniques share the general concept of trapping molecules between two contacting electrodes and thereby assembling metal–molecule–metal junctions for electrical probing. Through such measurements, as well as measurements on large-area junctions, it has become clear that many factors can influence the electrical current flow through molecular junctions, such as the intrinsic properties of molecules, electrodes, external environment, and so on.[8,9] So far, studies of single-molecular electrical properties have mainly focused on metal electrodes (Au, Ag, and Pt), largely due to the relative ease of their preparation and the ability to link molecules to these electrodes through a range of accessible chemisorption with a growing variety of anchoring groups (e.g., −SH, −NC, $-NH_2$, and −COOH).[10,11]

However, there is an increasing realization that new single-molecule electrical junction functionality can be achieved through the use of nonmetallic electrodes, with contacts such as indium–tin oxide (ITO),[12−15] carbon-based materials, and even novel two-dimensional (2D) graphene now being considered.[16−18] Kim et al. have formed graphite–molecules–Au molecular junctions by the use of the STM-BJ technique and measured the conductance of amine-terminated oligophenyl compounds.[19] Ullmann et al. presented a reliable fabrication of graphene molecular junctions with C_{60} end-capped molecular wires.[20] Dappe et al. combined carbon tips with graphene as a counter electrode to construct all-carbon molecular junctions.[21] These fundamental studies suggest that

Received: July 30, 2016
Revised: September 18, 2016
Published: September 26, 2016

DOI: 10.1021/acs.nanolett.6b03180
Nano Lett. 2016, 16, 6534−6540

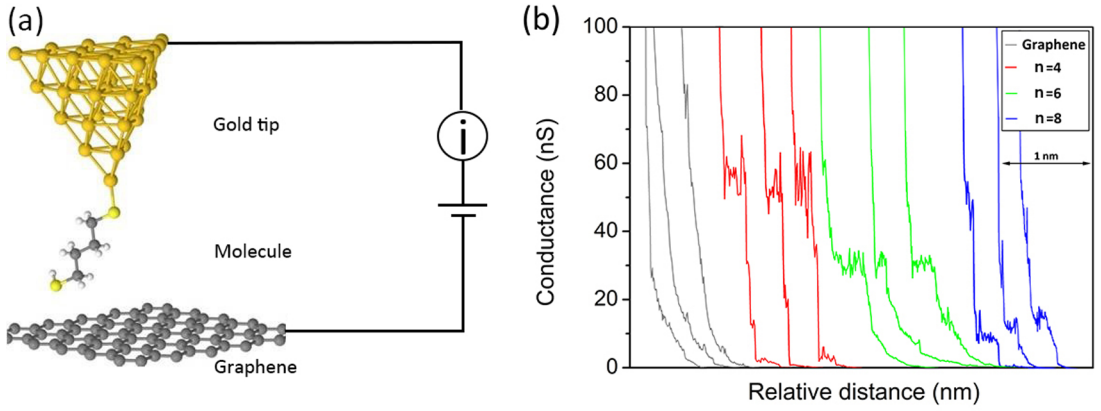

Figure 1. (a) Schematic diagram of the molecular junction formed in this study. (b) Typical $I(s)$ curves of bare graphene (gray, without molecular junctions formed), gold−1,4-butanedithiol−graphene junctions (red), gold−1,6-hexanedithiol−graphene junctions (green), and gold−1,8-octanedithiol−graphene junctions (blue).

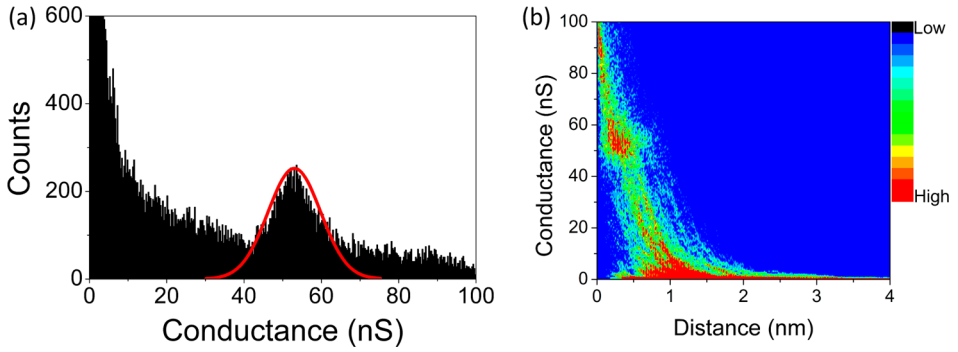

Figure 2. (a) 1D histograms of single-molecule conductance of gold−1,4-butanedithiol−graphene hybrid junctions with the Gaussian fit. (b) The corresponding 2D histogram with a sensitivity indicator of the conductance counts.

carbon based materials have the potential to be valuable alternative electrode materials for molecular electronics in the next generation of nanostructured devices.

Graphene, since its experimental discovery in 2004, has already been foreseen as an important future technology and applications of this material are gaining momentum.[22,23] This carbon monolayer exhibits remarkable electronic, thermal, mechanical and optical properties due to its zero-band gap and flat and super-thin structure,[24] making it useful as a platform for electronics, sensors, and electrodes in field effect transistors and as transparent contacts for photovoltaic devices.[25] Here, as a first step toward realizing its potential as electrodes, we demonstrate the use of graphene as a bottom electrode in place of the more commonly used gold. The well-studied system of thiol-terminated 1,*n*-alkane molecular bridges were selected as a test-bed to investigate the possibility to use graphene electrodes to form single molecule junctions. We have constructed gold-(1,*n*-alkanedithiol)-graphene hybrid junctions (n = 4, 6, 8, 10, 12) and measured the conductance of each molecular target using the so-called $I(s)$ STM method to form single molecule junctions.[6] In addition, we investigated the length dependence of conductance of these molecules with the decay constant (β_n) being experimentally determined across the n = 1 to 12 series, which we have compared with literature values for equivalent Au−molecule−Au junctions. Moreover, a combination of density functional theory (DFT) and a Keldysh−Green formalism for nonequilibrium systems was also used to determine the theoretical conductance values of each molecule and investigate the electrical properties.

First-principles theoretical methods have already been shown to be highly valuable in interpreting the transport properties of molecular electrical junctions[26,27] and have been developed as indispensable tools for understanding, in combination with experiments, junction electrical properties and mechanisms of charge transport.[28] Here, we show that the asymmetry of the junction and the combination of strong charge transfer at the gold electrode−molecule interface and weak coupling at the graphene bottom contact all play an important role in the electrical properties of the junctions. The combination of these factors leads to a strong reduction of the electronic length decay value, which is found to be about half of the value obtained for symmetric gold junctions. This lower attenuation factor leads to higher junction conductance for the longest junctions studied here.

As mentioned above, the $I(s)$ technique was used to construct gold−(1,*n*-alkanedithiol)−graphene hybrid junctions as well as to measure the single-molecule conductance (Figure 1a). Figure 1b shows two different kinds of typical conductance−distance curves: one type is the fast exponential decay (gray lines) of the current as a function of the distance between the tip and bare graphene substrate, and another type is the less-abrupt decay with the observation of well-defined plateaus (red, green, and blue lines). Taking 1,4-butanedithiol as an example, evidence for the formation of gold−1,4-butanedithiol−graphene hybrid junctions was derived from the observation of characteristic current plateaus located around 50−60 nS. Many factors can result in the sudden drop of the conductance in Figure 1b: one is the breaking of molecular

DOI: 10.1021/acs.nanolett.6b03180
Nano Lett. 2016, 16, 6534−6540

junctions, and another one can be the change of metal−molecule configurations during the withdrawal.[29,30] After the unbiased selection of plateaus featured curves, over 400 $I(s)$ curves were combined to form one-dimensional (1D) conductance and two-dimensional (2D) histograms, as shown in Figure 2. The 2D histograms were plotted by counting the data points corresponding to each conductance value as a function of the stretching distance of molecular junctions, and 1D histograms are represented by the conductance count values. From the 2D histograms, information concerning the distribution of conductance values and the length of the plateaus can be obtained, while the 1D histograms with peak fitting represent the conductance value. For each 2D histogram, a color bar was created to indicate the data sensitivity of conductance counts, with blue representing low count values, whereas red represents high count values. A significant peak around 53.0 nS is observed from the 1D histogram in Figure 2a, which indicates a dominant geometry between the molecules and the electrodes. Figure 2b is the corresponding 2D histogram with a distribution of conductance data ranging mainly between 45 and 60 nS. A red region (high point density) observed in the 2D histogram at the base of the 2D plot corresponds to the normal decay of the current, while the red region around 45−60 nS represents the distribution of current plateaus corresponding to molecular junctions. These values are consistent with the formation of molecular junctions for this molecule (Figure 1b).

Figure 3 presents conductance histograms of 1,n-alkanedithiol (n = 4, 6, 8, 10, 12) with the same conductance and

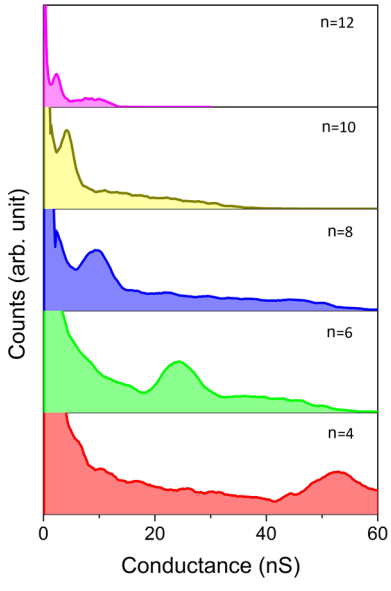

Figure 3. Conductance histograms for gold−n-alkanedithiol−graphene hybrid junctions in which n = 4 (red), 6 (green), 8 (blue), 10 (yellow), and 12 (magenta).

counts scale. A single main peak dominates each of these plots, and this indicates the respective conductance values for each molecular junction. We found the conductance values of 1,4-butanedithiol (red), 1,6-hexanedithiol (green), 1,8-octanedithiol (blue), 1,10-decanedithiol (yellow), and 1,12-dodecandithiol (magenta) to be 53.0, 24.3, 9.2, 4.2, and 2.3 nS, respectively (the corresponding 1D and 2D histogram with the Gaussian fit of each molecular junction are shown in the Supporting Information).

Also in parallel, we have calculated the theoretical conductance using a combined DFT and Keldysh−Green function formalism (Figure 4). In general, there is a good agreement between theoretical and experimental results despite some discrepancies in the overall behavior of the conductance, which can be attributed to different structural optimizations of the molecular junctions. Also, it is likely that many configurations are experimentally sampled in the stochastic junction formation process, whereas the calculations have been performed for an ideal single-molecule nanojunction. However, the general behavior compares well with experimental data. From Figure 4, we can observe that the molecular chains are oriented along the molecule−graphene axis for long chains, as expected, but present a small tilt angle for $n \leq 8$. This is probably related to a stronger tip−graphene interaction. With the shorter length of the molecule, the tip−graphene distance is much-reduced, therefore promoting more significant tip−graphene interactions, which can compress or tilt the molecule sandwiched in the junction.

Figure 5a shows the evolution of the electronic transmission, $T(E)$, for the different molecular lengths. These transmission curves show an important peak located at around −0.4 eV below the Fermi level for each molecular junction, which corresponds to the transmission resonance associated with the HOMO level. The position of the HOMO level, as also shown in the density of states (DOS) of the junction represented in Figure 5b, is an indication of the charge transfer between the molecule and the electrode. From our calculations, we determined that the charge transfer from the S atom in the S−Au contact is around −0.26 e. This charge transfer and the corresponding interface dipole are relatively small but significant enough still to partially depopulate the HOMO level and relocate it closer to the Fermi level.

The position of the HOMO here can be analyzed with respect to the case of the symmetric gold−molecule−gold junction. It is well-known that when a thiol-terminated molecule is adsorbed on gold, there is strong charge transfer from the sulfur to gold and that, consequently, the HOMO level generally shifts toward the Fermi level (adding charges to the molecule will push the HOMO further away from the Fermi level, whereas removing charges depopulates the HOMO level, forcing it toward the Fermi level). This charge transfer is driven by an interface electric dipole pointing from the sulfur to the gold. However, in the case of a molecular junction when the molecule is connected to two gold surfaces through thiol groups, the HOMO level is known to be located around 2 eV below the Fermi level.[31] This means that the charge transfer from the thiols to the gold surfaces is reduced, which can be interpreted as a cancellation of the two interface dipoles, which point in opposite directions, leading to an electrostatic equilibrium in the molecular junction. Now in the present case of our nonsymmetric gold−molecule−graphene junction, this equilibrium is broken. Indeed, the coupling between the thiol and the graphene is much weaker than the one between the thiol and gold due to van der Waals interactions. Therefore, the interface dipole on the graphene side is much smaller than on the gold side, meaning that the thiol−graphene dipole does not compensate the thiol−gold dipole. Thus, we recover a situation similar to the standard adsorption of a thiol terminated molecule on a gold surface, with a significant charge transfer at the thiol−gold interface, causing the HOMO level to move closer to the Fermi level. This is the reason why

DOI: 10.1021/acs.nanolett.6b03180
Nano Lett. 2016, 16, 6534−6540

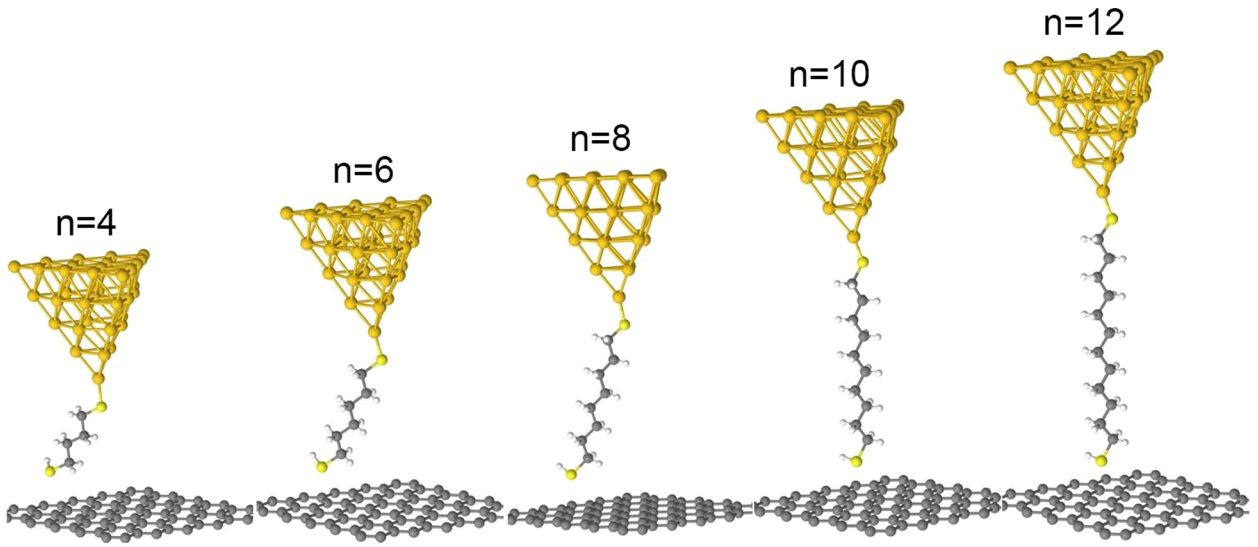

Figure 4. DFT-optimized model junctions used for the conductance calculations.

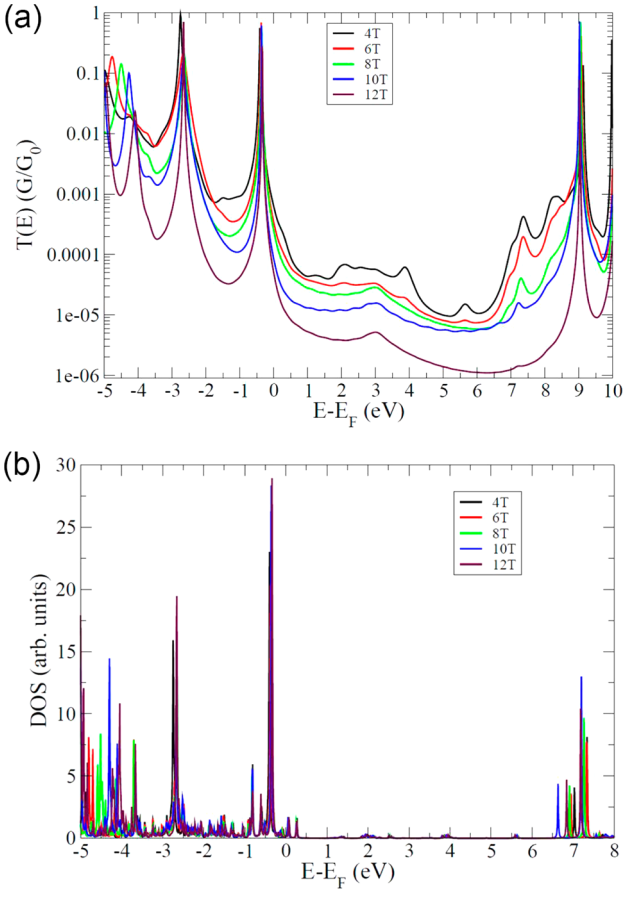

Figure 5. (a) Calculated electronic transmission $T(E)$ of the molecular junctions for the different lengths. (b) Calculated PDOS of the molecules in the molecular junctions for different lengths. In both figures, a strong resonance appears, associated with the HOMO level, at −0.4 eV with respect to the Fermi level.

we obtain a HOMO level and consequently a peak in the transmission at around −0.4 eV with respect to the Fermi level.

As the length increases, the molecular gap gets smaller leading to a decreasing HOMO − Fermi level energy difference. Notice that the difference between n = 8 and n = 10 is not so clear, probably due to the change of molecular conformation, from a tilted to a straight arrangement. As a remark, some small artifacts appear in the DOS due to the coupling with the gold electrode. As an atomic cluster, the gold tip presents many surface states that will couple with the molecule, which leads to the emergence of several peaks in the DOS. These peaks are not present in the electronic transmission because the coupling to the bulk electronic reservoirs removes these negligible contributions.

The results show a clear decrease in the single molecular conductance with the addition of methylene ($-CH_2$) units to the molecules. This phenomenon can be explained by a super-exchange mechanism. The exponential conductance decay with the number of molecular units is expressed by $G = A \exp(-\beta_n n)$, where G is the conductance; A is related to the nature of molecule−electrode interaction, which reflects the contact resistance; β_n is the decay constant, which describes the efficiency of electron transport through the molecules; and n is the number of methylene groups.[2,32] To investigate the relationship between molecular length and conductance, a linear fitting of the natural logarithmic single-molecule conductance versus the number of ($-CH_2$) units per molecular junction was plotted, and a decay constant β_n = 0.40 was obtained from the slope in Figure 6. Besides the experimental conductance values, the theoretical decay constant is estimated to be around β_n = 0.32, in good agreement with the experiments, confirming the importance of the molecule−graphene interface on the electronic transport.

Many literature studies have been performed to measure the single-molecule conductance and investigate the decay constant of gold−alkanedithiol−gold systems. For example, Marita and Lindsay measured the conductance of 1,n-alkanedithiol (n = 8, 10, 12) compounds using CP-AFM, with conductance values of 16.1 ± 1, 1.37 ± 0.35, and 0.35 ± 0.04 nS found, respectively.[33] Based on STM-BJ measurements, Li et al. have reported conductance values for 1,n-alkanedithiols of 19.4 (n = 8) and 1.6 nS (n = 10), for example.[34] In general, the decay constant (β_n) ranges from 0.8 to 1.0, measured by either STM-BJ or CP-AFM technologies.[33−35] Although the general trend of the conductance decay with molecular length is qualitatively similar in metallic and hybrid junctions, the comparison of absolute conductance values of these two junction types is not

DOI: 10.1021/acs.nanolett.6b03180
Nano Lett. 2016, 16, 6534−6540

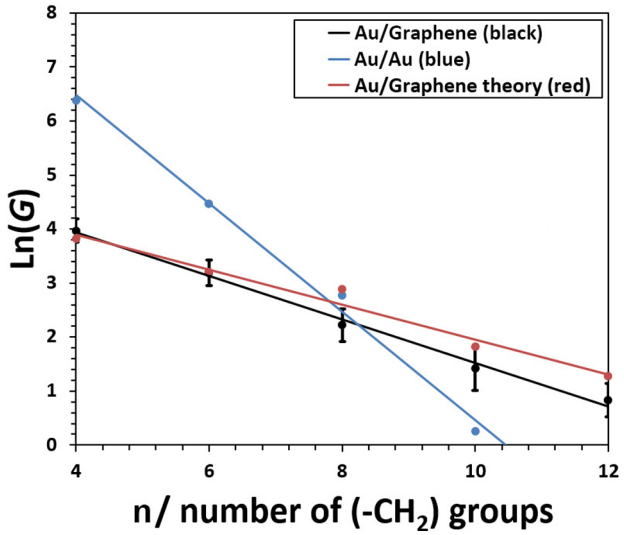

Figure 6. Natural logarithmic plot of the conductance as a function of the number of CH_2 groups. The red line represents the theoretical values, the black line is experimental data for Au−molecule−graphene junctions, and the blue line is the literature data[33] for Au−molecule−Au junctions.

straightforward, which is mainly due to the change of electrodes. This difference can be explained using a simple barrier tunneling model, which considers the relationship between the decay and the barrier height at the molecule−electrode interface:[28] $\beta_n = 2d_0\sqrt{(2m\varphi)/\hbar}$, where d_0 is the unit length between the monomers in the molecule, m is the mass of the electron, and φ is the barrier height. The latter is given by the energy difference between the Fermi level and the HOMO level of the molecule in the present case. In the case presented here, with our nonsymmetric junction between gold and graphene, the theoretically determined values are $\varphi \approx 0.4$ eV (see the DOS in Figure 5b) and $\beta_n = 0.4$. In the case of a symmetric gold junction where φ is significantly higher at ∼2 eV,[31] the corresponding β value would be $\beta_n = 0.4\sqrt{(2/0.4)} = 0.4\sqrt{(5)} = 0.9$, in good agreement with experimental observations. This simple reasoning shows that our findings are in good agreement with previous observations for Au−alkanedithiol−Au junctions. The contact resistance can be determined from the intercept of the linear fits in Figure 6 by extrapolating the fits of literature (blue line),[33] our experiments (black line), and theory (red line) to zero length, and the resistance values found are ∼27,[33] ∼5000, and ∼3900 kΩ, respectively. This shows that the contact resistance of Au−molecule−graphene junctions is much higher than for the Au−molecule−Au junctions. This difference indicates that the coupling between molecules and electrodes is rather weak at the graphene−molecule interface, which is in a good agreement with our theoretical interpretation above. The relatively small degree of electronic transfer at the graphene interface, in which the alkanedithiol donates a small partial electronic charge to the graphene surface, leads us to suggest that the binding at this interface is primarily related to a van der Waals coupling.[36]

It is useful to compare our results to those in which large area graphene contacts have been deployed. For example, Cao et al. have used graphene electrodes to create "robust and identical molecular transport junctions" using a lithographic method.[37] To further prove the effectiveness of their junctions, they capped molecules with amino groups to construct graphene−molecule−graphene symmetric junctions, which showed excellent reproducibility and stability. In addition, graphene−molecule−graphene symmetric molecular junctions were formed to create devices with electronic functionality (for example, reversible conductance switching based on graphene−azobenzene junctions).[38] The replacement of the gold electrode to construct a symmetric graphene−molecule−graphene junction changes the coupling strength between the molecules and electrodes.[25] In our present study we find that the bonding strength between graphene and thiol groups is relatively weak, and the interface resistance is much higher in comparison with that of the gold and thiol coupling. Thus, in graphene−alkanedithiol−graphene symmetric junctions, the resistance would be higher, giving a lower conductance than graphene−gold nonsymmetric junctions. It is therefore important to consider the nonsymmetric nature of the graphene−molecule−gold junctions and the complete junction electronic properties when comparing them to symmetric graphene−molecule−graphene junctions.

In the case of a symmetric gold−molecule−gold junction, the system tends to reach an electrostatic equilibrium where little charge transfer is observed, as explained earlier in the DOS analysis. However, in a nonsymmetric junction, substantial charge transfer is observed at the metallic electrode−molecule interface, which leads to a relocation of the HOMO closer to the Fermi level. In this case, there is large dipole at the gold−molecule interface that is not compensated at the graphene interface. Consequently, much-smaller attenuation of the current along the molecular wire is obtained. This effect is mainly due to the weak coupling at the molecule−graphene interface, which excludes any significant charge transfer at this interface.

Indeed, the effect of graphene is mainly to decouple the molecule from the second electrode and to favor a stronger charge transfer at the S−Au interface, hence relocating the HOMO level near the Fermi level. In this case, the effect is less due to the electronic properties of graphene than to the weak coupling associated with van der Waals interactions. Consequently, the combination of a weak coupling at the bottom graphene electrode with a strong coupling and high charge transfer at the top metallic electrode opens perspectives for controlling charge transfer and attenuation factors of single molecule junctions.

In summary, we have systematically studied using an STM-based technique the single-molecule conductance of 1,*n*-alkanedithiols (n = 4, 6, 8, 10, and 12) using graphene bottom and gold top electrodes. The conductance decays exponentially with the number of methylene groups with a decay constant of 0.40, much lower than the value obtained with a second metallic contact. Theoretical computations of the junction conductance values were also performed to investigate the electrical properties as a function of molecular length. These results show that the decay is related to the junction electronic structure, the nonsymmetric contact, and the weak coupling at the molecule−graphene interface, leading to a stronger charge transfer at the gold electrode−molecule interface. This work suggests that novel nonmetallic 2D materials could serve as promising electrodes to construct nonsymmetric junctions with tunable attenuation factors and electrical signatures, which differ from those of equivalent symmetric junctions with metal contacts.

DOI: 10.1021/acs.nanolett.6b03180
Nano Lett. 2016, 16, 6534−6540

Experimental and Theoretical Methodology. Graphene substrates (10 mm × 10 mm) were purchased from The Graphene Supermarket and consist of a few layer graphene layers on top of a nickel substrate. Raman spectroscopy (HORIBA Scientific) and STM (Bruker, EC-STM) were used to check the quality of each substrate. The STM tips were made by electrochemical etching of 0.25 mm diameter gold wires (Tianjing Lucheng Metal, 99.99%) in an electrolyte of hydrochloric acid and ethanol solution (50:50, v:v). Such tips were found to be suitable for high-spatial-resolution STM imaging.[39] 1,*n*-Alkanedithiols (n = 4, 6, 8, 10) were purchased from Alfa Aesar and used as received. 1,12-dodecanedithiol was synthesized in our lab and then characterized by nuclear magnetic resonance (Bruker, Topspin 400 MHz; see the detailed synthesis route and NMR spectra in the Supporting Information). Distilled water used in this experiment was supplied by an in-house purification system. Molecular adsorption to graphene substrate was generally achieved by immersing the qualified graphene substrate into molecular solutions (alkanedithiols−methanol, 1:20, v/v) for 90 s.

The STM based $I(s)$ technique was used to perform conductance measurements, and it was implemented according to the methodology described by Haiss et al. with necessary modifications to our Bruker STM equipment.[6] The gold STM tip was set at an initial vertical distance (4 nm in our experiment), and then the tip was brought close to the molecularly functionalized substrate by selecting a large current set-point (I_0) value. When the distance between the tip and substrate reached the preset threshold of the set-point current, the feedback loop was disconnected, the STM tip was then rapidly withdrawn to the initial vertical distance. During this process, the current was measured as a function of vertical distance. For each molecule, the parameters such as the applied bias, vertical distance, trigger threshold and moving speed can be varied. Over 2000 current−distance curves were collected, and those showing junction formation were selected on a consistent basis to avoid artificial bias. Then conductance histograms were constructed as described in the literature by combining these traces, and the resulting peaks in these plots for the selected molecules were used to compute molecular conductance.[4]

The molecular nanojunctions have also been studied theoretically, using the very efficient localized-orbitals basis set DFT code Fireball.[40] Basis sets of sp^3d^5 numerical orbitals for Au, sp^3 for C and S, and s for H have been used for structural optimization and conductance calculation of the nanojunctions, with cutoff radii (in atomic units) s = 4.5, p = 4.9, d = 4.3 (Au), s = 4.5, p = 4.5 (C), s = 3.1, p = 3.9 (S), and s = 4.1 (H).[41] The gold tip has been modeled by a pyramid of 35 Au atoms, terminating in a single apex.[42] We have considered a supercell of 5 × 5 C atoms in the XY plane for the graphene monolayer, on top of which we have set a molecule of defined length in the z direction, terminated by a connection with the Au pyramidal tip. The whole geometry has been optimized with Fireball until the forces reached a value below 0.05 eV/Å. A formalism taking into account van der Waals interactions has also been considered to determine the molecule−graphene distance.[43]

In a second step, we have used a nonequilibrium Keldysh−Green formalism, which takes multiple scattering into account to determine the conductance of the molecular junctions.[42] These values have then been computed for zero bias and at 0 K. However, in the calculations, we can modify the width of the electronic levels for the electrodes and for the molecule through an imaginary part in the corresponding self-energies.[44] Generally, they are more important for the electrodes to simulate the connection with a metallic surface rather than with a metallic cluster. This helps in particular in removing small peaks coming from local hybridization between the molecule and the electrode, which are introduced by the calculation but not visible experimentally. For the molecule, however, they are much smaller to clearly show the different resonances associated with the electronic levels of the molecule, like the HOMO, for example. In the present work, because we are interested in the evolution of the conductance with the molecular length, we have reduced this width to 0.002 eV to reduce the overlaps between the molecular levels and describe the molecule as a series of resonances rather than a molecular band. In the same manner, the imaginary parts for the gold tip and graphene have been set to 0.2 eV to enlarge the electronic levels due to the effect of a bulk behind the tip and the substrate not included in the simulation. Finally, it is noted that the bottleneck for the electronic transport in this junction is the weakly bonded molecule−graphene interface.

■ ASSOCIATED CONTENT

Supporting Information

The Supporting Information is available free of charge on the ACS Publications website at DOI: 10.1021/acs.nanolett.6b03180.

Figures showing the synthesis route of 1, 12-dodecanedithiol, NMR spectra, and detailed conductance histograms (1D, 2D) of 1,*n*-alkanedithiol (n = 6, 8, 10, 12) with Gaussian fit. (PDF)

■ AUTHOR INFORMATION

Corresponding Author

*E-mail: li.yang@xjtlu.edu.cn.

Author Contributions

L.Y., R.J.N., and C.Z. designed experiments; Q.Z., S.T., and C.W. carried out experiments; Q.Z and L.L. analyzed experimental results. C.G. and Y.J.D. conducted the simulation work and developed analysis tools. L.Y. and Y.J.D. wrote the manuscript with the input and approval from all the authors.

Funding

This work was supported by the National Natural Science Foundation of China (NSFC grants 21503169), the Jiangsu Science and Technology program (BK 20140405), Suzhou Industrial Park Initiative Platform Development for Suzhou Municipal Key Lab for New Energy Techniques (RR0140) and the XJTLU Research Development Fund (PGRS-13-01-03 and RDF-14-02-42). C.G. acknowledges funding by the Junta de Andalucía and the European Commission under the Co-Funding of the Seventh Framework Program in the People Program through the Andalusia Talent Hub program.

Notes

The authors declare no competing financial interest.

■ ACKNOWLEDGMENTS

We thank Dr. Eric Amigues for helping the synthesis of 1,12-dodecanedithiol.

■ REFERENCES

(1) Aviram, A.; Ratner, M. A. *Chem. Phys. Lett.* **1974**, *29*, 277−283.

DOI: 10.1021/acs.nanolett.6b03180
Nano Lett. 2016, 16, 6534−6540

(2) Chen, F.; Li, X.; Hihath, J.; Huang, Z.; Tao, N. J. *J. Am. Chem. Soc.* **2006**, *128*, 15874−15881.
(3) Reed, M. A. *Science* **1997**, *278*, 252−254.
(4) Xu, B.; Tao, N. J. *Science* **2003**, *301*, 1221−1223.
(5) Cui, X. D.; Primak, A.; Zarate, X.; Tomfohr, J.; Sankey, O. F.; Moore, A. L.; Moore, T. A.; Gust, D.; Harris, G.; Lindsay, S. M. *Nanotechnology* **2002**, *294*, 571−574.
(6) Haiss, W.; van Zalinge, H.; Higgins, S. J.; Bethell, D.; Höbenreich, H.; Schiffrin, D. J.; Nichols, R. J. *J. Am. Chem. Soc.* **2003**, *125*, 15294−15295.
(7) Nichols, R. J.; Haiss, W.; Higgins, S. J.; Leary, E.; Martin, S.; Bethell, D. *Phys. Chem. Chem. Phys.* **2010**, *12*, 2801−2815.
(8) Venkataraman, L.; Park, Y. S.; Whalley, A. C.; Nuckolls, C.; Hybertsen, M. S.; Steigerwald, M. L. *Nano Lett.* **2007**, *7*, 502−506.
(9) Scullion, L. E.; Leary, E.; Higgins, S. J.; Nichols, R. J. *J. Phys.: Condens. Matter* **2012**, *24*, 164211.
(10) Kiguchi, M.; Miura, S.; Takahashi, T.; Hara, K.; Sawamura, M.; Murakoshi, K. *J. Phys. Chem. C* **2008**, *112*, 13349−13352.
(11) Yokota, K.; Taniguchi, M.; Kawai, T. *J. Phys. Chem. C* **2010**, *114*, 4044−4050.
(12) Peng, Z.-L.; Chen, Z.-B.; Zhou, X.-Y.; Sun, Y.-Y.; Liang, J.-H.; Niu, Z.-J.; Zhou, X.-S.; Mao, B.-W. J. *J. Phys. Chem. C* **2012**, *116*, 21699−21705.
(13) Battacharyya, S.; Kibel, A.; Kodis, G.; Liddell, P. A.; Gervaldo, M.; Gust, D.; Lindsay, S. *Nano Lett.* **2011**, *11*, 2709−2714.
(14) Chen, F.; Hihath, J.; Huang, Z.; Li, X.; Tao, N. J. *Annu. Rev. Phys. Chem.* **2007**, *58*, 535−564.
(15) Kim, B.; Choi, S. H.; Zhu, X. Y.; Frisbie, C. D. *J. Am. Chem. Soc.* **2011**, *133*, 19864−19877.
(16) Jia, C.; Ma, B.; Xin, N.; Guo, X. *Acc. Chem. Res.* **2015**, *48*, 2565−2575.
(17) Pshenichnyuk, I. A.; Coto, P. B.; Leitherer, S.; Thoss, M. *J. Phys. Chem. Lett.* **2013**, *4*, 809−814.
(18) Liu, L.; Zhang, Q.; Tao, S.; Zhao, C.; Almutib, E.; Al-Galiby, Q.; Bailey, S. W. D.; Grace, I.; Lambert, C. J.; Du, J.; Yang, L. *Nanoscale* **2016**, *8*, 14507−14513.
(19) Kim, T.; Liu, Z.-F.; Lee, C.; Neaton, J. B.; Venkataraman, L. *Proc. Natl. Acad. Sci. U. S. A.* **2014**, *111*, 10928−10932.
(20) Ullmann, K.; Coto, P. B.; Leitherer, S.; Molina-Ontoria, A.; Martín, N.; Thoss, M.; Weber, H. B. *Nano Lett.* **2015**, *15*, 3512−3518.
(21) Dappe, Y. J.; Gonzalez, C.; Cuevas, J. C. *Nanoscale* **2014**, *6*, 6953−6958.
(22) Wen, Y.; Chen, J.; Guo, Y.; Wu, B.; Yu, G.; Liu, Y. *Adv. Mater.* **2012**, *24*, 3482−3485.
(23) Järvinen, P.; Hämäläinen, S. K.; Banerjee, K.; Häkkinen, P.; Ijäs, M.; Harju, A.; Liljeroth, P. *Nano Lett.* **2013**, *13*, 3199−3204.
(24) Bolotin, K. I.; Sikes, K. J.; Jiang, Z.; Klima, M.; Fudenberg, G.; Hone, J.; Kim, P.; Stormer, H. L. *Solid State Commun.* **2008**, *146*, 351−355.
(25) Jia, C.; Guo, X. *Chem. Soc. Rev.* **2013**, *42*, 5642−5660.
(26) Rocha, A. R.; Garcia-suarez, V. M.; Bailey, S. W.; Lambert, C. J.; Ferrer, J.; Sanvito, S. *Nat. Mater.* **2005**, *4*, 335−339.
(27) Quek, S. Y.; Venkataraman, L.; Choi, H. J.; Louie, S. G.; Hybertsen, M. S.; Neaton, J. B. *Nano Lett.* **2007**, *7*, 3477−3482.
(28) Cuevas, J. C.; Scheer, E. *Molecular Electronics: an Introduction to Theory and Experiment*; World Scientific: Singapore, 2010.
(29) Nazin, G. V.; Qiu, X. H.; Ho, W. *Science* **2003**, *302*, 77−81.
(30) Basch, H.; Cohen, R.; Ratner, M. A. *Nano Lett.* **2005**, *5*, 1668−1675.
(31) González, M. T.; Brunner, J.; Huber, R.; Wu, S.; Schönenberger, C.; Calame, M. *New J. Phys.* **2008**, *10*, 065018.
(32) Wang, Y.-H.; Zhou, X.-Y.; Sun, Y.-Y.; Han, D.; Zheng, J.-F.; Niu, Z.-J.; Zhou, X.-S. *Electrochim. Acta* **2014**, *123*, 205−210.
(33) Morita, T.; Lindsay, S. J. *J. Am. Chem. Soc.* **2007**, *129*, 7262−7263.
(34) Li, X.; He, J.; Hihath, J.; Xu, B.; Lindsay, S. M.; Tao, N. J. *J. Am. Chem. Soc.* **2006**, *128*, 2135−2141.
(35) Jang, S.-Y.; Reddy, P.; Majumdar, A.; Segalman, R. A. *Nano Lett.* **2006**, *6*, 2362−2367.
(36) Adak, O.; Kladnik, G.; Bavdek, G.; Cossaro, A.; Morgante, A.; Cvetko, D.; Venkataraman, L. *Nano Lett.* **2015**, *15*, 8316−8321.
(37) Cao, Y.; Dong, S.; Liu, S.; He, L.; Gan, L.; Yu, X.; Steigerwald, M. L.; Wu, X.; Liu, Z.; Guo, X. *Angew. Chem.* **2012**, *124* (49), 12394−12398.
(38) Cao, Y.; Dong, S.; Liu, S.; Liu, Z.; Guo, X. *Angew. Chem., Int. Ed.* **2013**, *52*, 3906−3910.
(39) Ren, B.; Picardi, G.; Pettinger, B. *Rev. Sci. Instrum.* **2004**, *75*, 837.
(40) Lewis, J. P.; Jelínek, P.; Ortega, J.; Demkov, A. A.; Trabada, D. G.; Haycock, B.; Wang, H.; Adams, G.; Tomfohr, J. K.; Abad, E.; Wang, H.; Drabold, D. A. *Phys. Status Solidi B* **2011**, *248*, 1989−2007.
(41) Basanta, M. A.; Dappe, Y. J.; Jelínek, P.; Ortega, J. *Comput. Mater. Sci.* **2007**, *39*, 759−766.
(42) Reecht, G.; Bulou, H.; Scheurer, F.; Speisser, V.; Mathevet, F.; González, C.; Dappe, Y. J.; Schull, G. *J. Phys. Chem. Lett.* **2015**, *6*, 2987−2992.
(43) Dappe, Y. J.; Ortega, J.; Flores, F. *Phys. Rev. B: Condens. Matter Mater. Phys.* **2009**, *79*, 165409.
(44) González, C.; Abad, E.; Dappe, Y. J.; Cuevas, J. C. *Nanotechnology* **2016**, *27*, 105201.

DOI: 10.1021/acs.nanolett.6b03180
Nano Lett. 2016, 16, 6534−6540